Acta Crystallographica Section B
Structural Science
ISSN 0108-7681

addenda and errata

$[Ru(py)_4Cl(NO)](PF_6)_2\cdot 0.5H_2O$: a model system for structural determination and *ab initio* calculations of photo-induced linkage NO isomers. Erratum

Benoît Cormary,[a,b] Isabelle Malfant,[a,b]* Lydie Valade,[a] Marylise Buron-Le Cointe,[c] Loïc Toupet,[c] Teodora Todorova,[c] Bernard Delley,[d] Dominik Schaniel,[e] Nicholas Mockus,[e] Theo Woike,[e]* Karla Fejfarová,[f] Václav Petříček[f] and Michal Dušek[f]

[a]CNRS-LCC (Laboratoire de Chemie de Coordination), 205 route de Narbonne F-31077 Toulouse, France, [b]Université de Toulouse, UPS, INPT, LCC, F-31077 Toulouse, France, [c]Institut de Physique de Rennes, UMR UR1-CNRS 6251, Université de Rennes 1, 35042 Rennes, France, [d]Condensed Matter Theory, Paul Scherrer Institut, 5232 Villigen PSI, Switzerland, [e]Physikalisches Institut, Universität zu Köln, Zülpicher Strasse 77, 50937 Köln, Germany, and [f]Institute of Physics, Acadmy of Sciences of the Czech Republic, Na Slovance 2, 18221 Praha 8, Czech Republic

Correspondence e-mail: isabelle.malfant@lcc-toulouse.fr, th.woike@uni-koeln.de

In the paper by Cormary *et al.* [*Acta Cryst.* (2009), B**65**, 612–623] two authors were inadvertently omitted from the author list and one name was given incorrectly.

In the paper by Cormary *et al.* [*Acta Cryst.* (2009), B**65**, 612–623] two authors were inadvertently omitted from the author list. The missing authors are Lydie Valade and Teodora Todorova. Also, the name of one of the authors was given incorrectly. The correct name should be Marylise Buron-Le Cointe. The complete list of authors is given above.

References

Cormary, B., Malfant, I., Buron-Le Cointe, M., Toupet, L., Delley, B., Schaniel, D., Mockus, N., Woike, T., Fejfarová, K., Petříček, V. & Dušek, M. (2009). *Acta Cryst.* B**65**, 612–623.

 doi:10.1107/S0108768109044899

Acta Crystallographica Section B
Structural Science
ISSN 0108-7681

$[Ru(py)_4Cl(NO)](PF_6)_2\cdot 0.5H_2O$: a model system for structural determination and *ab initio* calculations of photo-induced linkage NO isomers

Benoît Cormary,[a,b] Isabelle Malfant,[a,b]* Marylize Buron-Le Cointe,[c] Loïc Toupet,[c] Bernard Delley,[d] Dominik Schaniel,[e] Nicholas Mockus,[e] Theo Woike,[e]* Karla Fejfarová,[f] Václav Petříček[f] and Michal Dušek[f]

[a]CNRS-LCC (Laboratoire de Chimie de Coordination), 205 route de Narbonne F-32077 Toulouse, France, [b]Université de Toulouse, UPS, INPT, LCC, F-32077 Toulouse, France, [c]Institut de Physique de Rennes, UMR UR1-CNRS 6251, Université de Rennes 1, 35042 Rennes, France, [d]Condensed Matter Theory, Paul Scherrer Institut, 5232 Villigen PSI, Switzerland, [e]Physikalisches Institut, Universität zu Köln, Zülpicher Strasse 77, 50937 Köln, Germany, and [f]Institute of Physics, Academy of Sciences of the Czech Republic, Na Slovance 2, 18221 Praha 8, Czech Republic

Correspondence e-mail: isabelle.malfant@lcc-toulouse.fr, th.woike@uni-koeln.de

Received 17 April 2009
Accepted 10 July 2009

Structure analysis of ground state (GS) and two light-induced (SI and SII) metastable linkage NO isomers of $[Ru(py)_4Cl(NO)](PF_6)_2\cdot 0.5H_2O$ is presented. Illumination of the crystal by a laser with $\lambda = 473$ nm at $T = 80$ K transfers around 92% of the NO ligands from Ru—N—O into the isomeric configuration Ru—O—N (SI). A subsequent irradiation with $\lambda = 980$ nm generates about 48% of the side-on configuration $Ru<^{N}_{O}$ (SII). Heating to temperatures above 200 K or irradiation with light in the red spectral range transfers both metastable isomers reversibly back to the GS. Photodifference maps clearly show the N—O configurations for both isomers and they could be used to find a proper starting model for subsequent refinements. Both metastable isomers have slightly but significantly different cell parameters with respect to GS. The main structural changes besides the Ru—O—N and $Ru<^{N}_{O}$ linkage are shortenings of the *trans* Ru—Cl bonds and the equatorial Ru—N bonds. The experimental results are compared with solid-state calculations based on density functional theory (DFT), which reproduce the observed structures with high accuracy concerning bond lengths and angles. The problem of how the different occupancies of SI and GS could affect refinement results was solved by a simulation procedure using the DFT data as starting values.

1. Introduction

The aim of photocrystallography is the determination of structures and hence atomic positions, which are changed upon light irradiation. In transition metal compounds, light-induced charge-transfer transitions alter the electron density on the central atom and in the bonding or antibonding orbitals of the ligands. If such a rearrangement opens an instability for the nuclear positions of some ligands and the lifetime of the induced electron density is sufficiently long with respect to nuclear movements, isomers can be formed as new metastable structures. In the static case, *i.e.* when the light-induced structural change is long-lived and thus suitable for collection of X-ray or neutron datasets, the structure of the ground state and the final relaxed light-induced state can be determined (Pillet *et al.*, 2008; Varret *et al.*, 2008; Schefer *et al.*, 2008; Coppens *et al.*, 2008). However, the atomic positions in the two states need to be sufficiently separate and the population, *i.e.* the number of excited species, needs to be large enough. In the dynamic case the movement of the atoms is directly followed with time-resolved diffraction methods or X-ray absorption spectroscopy in the femto- and picosecond range, such that under suitable conditions intermediate excited states can also be structurally detected (Collet *et al.*, 2008; Korff Schmising *et al.*, 2008; Bressler *et al.*, 2008).

In many substances, phase transitions (Nasu, 2004) or photochemical reactions can be triggered by light of a suitable wavelength. As a consequence of light irradiation novel atomic positions are adopted, ligand groups are separated and novel isomeric configurations are built. Of special interest for the field of reversible photochemistry, *i.e.* the generation of chemical complexes which are not accessible by standard synthetic routes, is the photogeneration of reversible isomeric configurations or ligand transfers. This long-known phenomenon, *e.g.* in $[Co(NH_3)_5NO_2]^{2+}$ (Werner, 1907; Kubota & Ohba, 1992) allows for the generation of novel substances by light irradiation. Using photocrystallography it was found that in ions of the type $[ML_yZ]^n$ the photoactive ligands Z = NO, NO_2, N_2, SO, SO_2, SO_3, NCS *etc.* can adopt novel linkage isomeric configurations, *e.g.* M—N—O switches to M—O—N or M—S—O to M—O—S *etc.* (Carducci *et al.*, 1997; Schaniel *et al.*, 2005, 2006; Bowes *et al.*, 2006; Fomitchev *et al.*, 2000; Kovalevsky *et al.*, 2005; Rachford *et al.*, 2005). The central atom M = Fe, Ru, Os, Ni, Re, Pt *etc.* and the ligands L_y (*e.g.* Cl, CN, NH_3, NO_2 *etc.*) can be chosen almost arbitrarily (Zöllner *et al.*, 1989; Ookubo *et al.*, 1996; Gütlich *et al.*, 2001; Coppens *et al.*, 2002; Bitterwolf, 2004; Schaniel, Woike *et al.*, 2007). Fig. 1 shows well the ground state and two such metastable linkage isomer configurations in the prototypical complex $[Fe(CN)_5NO]^{2-}$. Light irradiation in the blue–green spectral range at temperatures below 150 K can transfer about 50% of the Fe—N—O (GS) into the Fe—O—N (SI) configuration and about 2% into the SII configuration. Subsequent irradiation with light in the near IR spectral range (maximum at 1064 nm) generates about 30% of SII and 70% of GS. The N—O ligand has an eclipsed position, *i.e.* N and O are located over the C atoms of the equatorial CN^- ligands, and due to the *m* site symmetry there are two N—O positions related by the mirror plane.

Using photocrystallography, many such light-induced structures have been solved with X-ray or neutron diffraction at low temperatures (Grenthe & Nordin, 1979; Carducci *et al.*, 1997; Coppens *et al.*, 2002; Cole, 2004; Schaniel *et al.*, 2005, 2006). In these investigations a fundamental problem needs to be solved; in general, only a fraction of the molecules can be transferred to the metastable state. The reason for this incomplete transferability is found in the absorption cross sections of ground (GS) and metastable states (MS), $\sigma_{GS}(\lambda)$ and $\sigma_{MS}(\lambda)$, since a spectral overlap of the corresponding absorption bands at the irradiation wavelength λ results in back and forth transfers between GS and MS, and thus leads to an equilibrium between GS and MS determined essentially by the ratio $\sigma_{GS}(\lambda)/\sigma_{MS}(\lambda)$. If these bands are sufficiently separated as is known for the optically induced low-spin high-spin transitions (Hauser, 1991; Gütlich *et al.*, 2004; Legrand *et al.*, 2005) and irreversible photoinduced dimerizations (Nakanishi *et al.*, 1981), 100% of the molecules can be transferred. Here the absorption bands of GS and MS are sufficiently separated such that at the population wavelength λ no back transfer from MS to GS occurs. The population of the photogenerated molecules can be considered in the structure factor F by a population factor P according to

$$F = (1 - P)F_{GS} + PF_{MS} + F_{rest} \quad (1)$$

with $0 \leq P \leq 1$. F_{GS} and F_{MS} are the structure factors of the ground state (GS) and the metastable state (MS), respectively. F_{rest} describes the part of the crystal which remains unaffected by the irradiation, *e.g.* crystal water or counter ions. The ground state and F_{rest} are determined before irradiation, such that one needs to refine only F_{GS} and F_{MS} after irradiation, where F_{GS} does not suffer significant changes after the irradiation. The new structure of ions in MS can alter the lattice constants, but will not influence the structure of ions in GS. However, at low populations one needs to introduce further constraints, which hamper a complete structural refinement. For example, for local structural changes of a ligand (*e.g.* M—N—O $\Rightarrow$ M—O—N) the positions and displacement parameters of all other atoms within the molecule need to be fixed at ground state positions. Only the parameters in the M—N—O area are refined. For sufficiently high populations the parameters of the *trans* ligand can also be refined. Helpful for such mixed refinements of GS and MS species are rigid-body constraints and assumptions on split positions of photoactive ligands (Carducci *et al.*, 1997). While these assumptions allow the main features to be determined, they obviously lead to an incomplete picture of the photo-induced structural change, since the whole molecule relaxes after an electronic excitation and reconfiguration. Helpful in this context are simulations of the local structural changes as a function of population number in order to find whether the novel structure can be detected with the planned measurement (Schefer *et al.*, 2008). An important tool to further identify and determine light-induced structural changes is density functional theory (DFT) calculations (Delley *et al.*, 1997; Coppens *et al.*, 2002; Delley, 2008; Ishikawa & Tanaka, 2008; Sizova *et al.*, 2008). The validity of such calculations depends on the functional used and whether they are performed only for the molecular ion with an assumed charge background for charge compensation or whether they are made for all atoms in the complete solid state.

All of these problems concerning refinement can be avoided if the system can be photoswitched at nearly 100%. This allows for a complete structural analysis of the MS, the same as known for standard structures (*i.e.* GS) and yields insight into the errors possibly made during refinements of

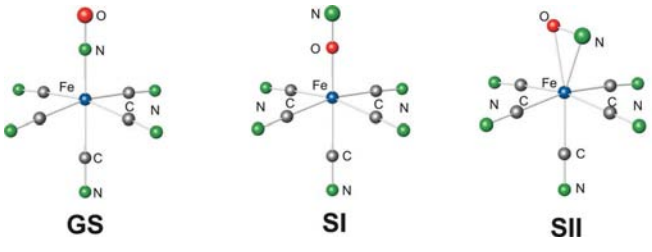

Figure 1
Ground state GS, isonitrosyl configuration SI, and side-on configuration SII of the $[Fe(CN)_5NO]^{2-}$ ion after irradiation at T = 100 K with λ = 458 nm for SI and subsequent irradiation with 1064 nm for generation of SII.

Table 1
Experimental and refinement details.

	Ground state	SI	SII
Crystal data			
Chemical formula	$2(C_{20}H_{20}ClN_5ORu)\cdot4PF_6\cdot H_2O$	$2(C_{20}H_{20}ClN_5ORu)\cdot4PF_6\cdot H_2O$	$2(C_{20}H_{20}ClN_5ORu)\cdot4PF_6\cdot H_2O$
M_r	1563.8	1563.8	1563.8
Cell setting, space group	Monoclinic, $P2_1/c$	Monoclinic, $P2_1/c$	Monoclinic, $P2_1/c$
Temperature (K)	100	100	100
a, b, c (Å)	15.7016 (4), 13.4512 (4), 26.8147 (7)	15.7224 (4), 13.3917 (4), 26.7648 (7)	15.7444 (7), 13.4456 (7), 26.8410 (10)
β (°)	92.436 (2)	92.603 (2)	92.195 (4)
V (Å^3)	5658.3 (3)	5629.5 (3)	5677.9 (5)
Z	8	8	8
Radiation type	Mo $K\alpha$	Mo $K\alpha$	Mo $K\alpha$
μ (mm^{-1})	0.869	0.872	0.866
Crystal form, size (mm)	Parallelepiped, 0.2 × 0.2 × 0.2	Parallelepiped, 0.2 × 0.2 × 0.2	Parallelepiped, 0.2 × 0.2 × 0.2
Data collection			
Diffractometer	Oxford Diffraction Xcalibur 3 with a two-dimensional sapphire 3 CCD detector	Oxford Diffraction Xcalibur 3 with a two-dimensional sapphire 3 CCD detector	Oxford Diffraction Xcalibur 3 with a two-dimensional sapphire 3 CCD detector
Data collection method	Full sphere 32, detector distance 50 mm	Full sphere 32, detector distance 50 mm	ω scan, 138 images of 0.75 width in omega
Absorption correction	None	None	None
No. of measured, independent and observed reflections	52 213, 18 099, 11 336	58 320, 18 723, 11 569	54 103, 18 423, 4376
Criterion for observed reflections	$I>3\sigma(I)$	$I>3\sigma(I)$	$I>3\sigma(I)$
R_{int}	0.033	0.042	0.095
θ_{max} (°)	32.1	33.7	32.1
Refinement			
Refinement on	F	F	F
$R[F^2>2\sigma(F^2)]$, $wR(F^2)$, S	0.031, 0.032, 1.22	0.029, 0.027, 1.10	0.035, 0.031, 0.55
No. of reflections	18 099	18 723	54 103
No. of parameters	768	775	766
H-atom treatment	Mixture†	Mixture†	Mixture†
$(\Delta/\sigma)_{max}$	0.036	0.043	0.046
$\Delta\rho_{max}$, $\Delta\rho_{min}$ (e Å^{-3})	1.25, −0.93	0.66, −0.76	0.58, −0.35
Extinction method	B–C type 1 Lorentzian isotropic (Becker & Coppens, 1974)	B–C type 1 Lorentzian isotropic (Becker & Coppens, 1974)	None
Extinction coefficient	400 (400)	1200 (300)	–

Computer programs used: *CrysAlis CCD* (Oxford Diffraction, 2007*a*), *CrysAlis RED* (Oxford Diffraction, 2007*b*), *SHELXS*97 (Sheldrick, 2008), *JANA*2006 (Petříček *et al.*, 2006), *DIAMOND* (Brandenburg & Putz, 2005). † Mixture of independent and constrained refinement.

incompletely switched structures owing to the necessary constraints. Of special interest is the question whether the determination of bond lengths depends on the amount of population.

Therefore, we report on the complete structural analysis of the ground state and two light-induced metastable states SI and SII in $[Ru(py)_4Cl(NO)](PF_6)_2\cdot0.5H_2O$ (py = pyridine: NC_5H_5). In this compound SI can be populated to ∼ 92% and SII to ∼ 48%. Owing to these high population numbers the principal questions raised above about photocrystallographic experiments can be discussed and analyzed in detail. Especially the quality of structural determinations for populations less than 50%, which include many necessary constraints, are discussed. The ground-state structure of $[Ru(py)_4Cl(NO)](PF_6)_2\cdot0.5H_2O$ was determined earlier by Kimura *et al.* (1983), yielding an R value of $wR_{(all)}$ = 0.0551 without refining H atoms. As a further important result we present DFT calculations on the ground and metastable states SI and SII of the solid state, which show the high level of accuracy that can be reached nowadays for the prediction of structures. State-of-the-art DFT calculations agree with each other by no better than 0.01 Å for the length of chemical bonds when the same functional is used consistently. For challenging compounds as studied here agreement of theory with experiment for bond lengths is expected to be better than 0.03 Å because of limitations inherent to popular, practicable density-functional approximations.

2. Experimental

$[Ru(py)_4Cl(NO)](PF_6)_2\cdot1/2\ H_2O$ was prepared as previously described (Bottomley & Mukaida, 1982; Schaniel, Cormary *et al.*, 2007). Orange single crystals were grown by slow evaporation of a CH_3CN plus H_2O solution at T = 298 K.

For X-ray diffraction experiments a $[Ru(py)_4Cl(NO)](PF_6)_2\cdot0.5H_2O$ single crystal with a diameter of 190 µm was

Table 2
Selected bond distances (Å) and angles (°) in GS, SI and SII from X-ray refinement and solid-state DFT calculations.

	GS		SI		SII	
Distance/angle	X-ray	DFT	X-ray	DFT	X-ray	DFT
Ru1—Cl1	2.3206 (6)	2.3409	2.2782 (5)	2.3015	2.3045 (8)	2.3217
Cl1—Ru1—N5	178.96 (6)	179.17	–	–	158.4 (4)	157.22
Cl1—Ru1—O5	–	–	178.93 (4)	178.98	171.1 (5)	170.34
Ru1—N5	1.7550 (17)	1.7848	–	–	1.921 (13)	1.9774
Ru1—N5—O5	178.30 (16)	178.48	–	–	87.3 (9)	85.12
N5—Ru1—O5	–	–	–	–	30.2 (6)	32.23
Ru1—O5	–	–	1.8630 (13)	1.9036	2.144 (14)	2.2184
Ru1—O5—N5	–	–	178.12 (12)	179.04	63.4 (9)	62.64
Ru1—N1	2.1044 (17)	2.1388	2.0949 (13)	2.1241	2.099 (2)	2.1354
Ru1—N2	2.1041 (17)	2.1299	2.0958 (14)	2.1192	2.086 (2)	2.1154
Ru1—N3	2.1069 (18)	2.1311	2.0932 (14)	2.1344	2.111 (3)	2.1714
Ru1—N4	2.1142 (17)	2.1493	2.1023 (14)	2.1209	2.108 (2)	2.1424
N5—O5	1.146 (2)	1.1520	1.140 (2)	1.1514	1.08 (2)	1.1875
Ru2—Cl2	2.3231 (5)	2.3366	2.2798 (5)	2.2950	2.2967 (8)	2.3141
Cl2—Ru2—N10	175.47 (6)	175.09	–	–	160.8 (2)	155.77
Cl2—Ru2—O10	–	–	175.73 (4)	175.63	173.18 (16)	171.80
Ru2—N10	1.7537 (16)	1.7818	–	–	1.982 (6)	1.9659
Ru2—N10—O10	172.42 (16)	172.36	–	–	87.6 (5)	85.14
N10—Ru2—O10	–	–	–	–	25.5 (3)	32.43
Ru2—O10	–	–	1.8619 (12)	1.8962	2.153 (6)	2.2097
Ru2—O10—N10	–	–	171.43 (13)	173.22	66.9 (5)	62.43
Ru2—N6	2.1213 (16)	2.1507	2.1061 (13)	2.1363	2.117 (3)	2.1421
Ru2—N7	2.1051 (17)	2.1367	2.0954 (15)	2.1252	2.103 (3)	2.1389
Ru2—N8	2.1036 (16)	2.1365	2.0900 (13)	2.1227	2.102 (2)	2.1231
Ru2—N9	2.1050 (17)	2.1334	2.0930 (15)	2.1246	2.110 (2)	2.1630
N10—O10	1.147 (2)	1.1520	1.142 (2)	1.1497	0.928 (9)	1.1892

Figure 2
Color change of $[Ru(py)_4Cl(NO)](PF_6)_2{\cdot}0.5H_2O$ upon irradiation with laser light of wavelengths 473 and 980 nm.

mounted on a glass needle and adjusted on the four-circle Oxford Diffraction Xcalibur 3 diffractometer (Mo $K\alpha$ radiation) with a two-dimensional sapphire 3 CCD detector, equipped with an Oxford Cryosystems nitrogen-flow cryostat allowing a control of ± 0.1 K at 80 K. The unit-cell parameters and the data reduction were obtained with *CrysAlis* software (Oxford Diffraction, 2007*a*,*b*). After collection of the ground-state dataset, the crystal was illuminated with λ = 473 nm for 1 h using a light intensity of 400 mW cm^{-2}, in order to reach saturation at a total exposure of 1440 J cm^{-2}. In order to reduce a possible significant depopulation of metastable states by X-ray irradiation, as reported in Pressprich *et al.* (1994), we had to reduce the exposure time of X-rays. Nevertheless, data up to $\sin\theta/\lambda \simeq 0.75$ Å^{-1} were collected for GS and SI.

SII was generated by subsequent illumination of SI with a laser diode at λ = 980 nm having light intensity of 60 mW cm^{-2} for 30 min. After the transfer SI ⇒ SII the depopulation from SII into GS occurs (Schaniel, Cormary *et al.*, 2007). The data collection was again made up to $\sin\theta/\lambda \simeq 0.75$ Å^{-1}. However, owing to the shorter measurement time we observed only ∼4000 observed reflections having $I > 3\sigma(I)$.

All measurements were performed with the same single crystal. The lifetime τ of SI and SII at 110 K is $\tau = 5.9 \times 10^{19}$ s (1.8×10^{12} years) and $\tau = 3.7 \times 10^{7}$ s (1.1 years), respectively, such that a possible decay of the metastable states during the data collection can occur only by the X-ray radiation as is shown in Pressprich *et al.* (1994). The lifetime τ is calculated from the activation energy E_a and the frequency factor Z known from DSC measurements [E_a = 0.70 eV (SI), E_a = 0.38 eV (SII); $Z = 2 \times 10^{12}$ s^{-1}(SI), 7×10^{9} s^{-1} (SII)] using the Arrhenius equation $1/\tau = Z \exp(-E_a/k_BT)$ (Schaniel, Cormary *et al.*, 2007).

Data collection parameters are summarized in Table 1. The space group $P2_1/c$ of the studied crystal remains identical for the three states, but all unit-cell parameters change significantly when going from GS ⇒ SI ⇒ SII. The lattice constant a for SI increases with respect to GS by 0.13% and by 0.27% in SII, while b decreases by 0.44% (SI) and by 0.04% (SII,) and c decreases in SI by 0.19% and increases in SII by 0.09%. The monoclinic angle β is larger in SI by 0.167° and smaller in SII by 0.241° with respect to GS. The change in the lattice parameters is the first indication of a structural response upon light illumination. Furthermore, the color of the crystal changes from orange in GS to green in SI and to black in SII, as illustrated in Fig. 2. The color changes are due to the increase of new absorption bands in the visible spectral range (Schaniel, Cormary *et al.*, 2007).

3. Refinement and DFT calculations

Structural refinement of all three states (GS, SI and SII) was performed with the program package *JANA*2006 and in all these refinements the hydrogen positions were fixed by applying ideal geometrical conditions.

Table 3
Selected torsion angles in (°) GS, SI and SII from X-ray refinement and DFT calculations.

	GS		SI		SII	
Torsion angle	X-ray	DFT	X-ray	DFT	X-ray	DFT
C1—N1—N3—C11	92.5 (2)	92.05	91.99 (18)	91.58	88.7 (3)	83.10
C1—N1—N3—C15	−89.9 (2)	−92.05	−90.07 (19)	−91.51	−94.4 (3)	−100.90
C5—N1—N3—C11	−90.0 (2)	−91.91	−91.23 (18)	−91.59	−90.4 (3)	−96.32
C5—N1—N3—C15	87.6 (2)	83.96	86.71 (18)	85.30	86.5 (3)	79.65
C6—N2—N4—C16	99.4 (2)	96.16	99.26 (17)	96.78	98.9 (3)	98.15
C6—N2—N4—C20	−81.6 (2)	−82.58	−80.77 (17)	−82.91	−81.3 (3)	−79.42
C10—N2—N4—C16	−77.4 (2)	−79.26	−78.55 (17)	−79.44	−78.1 (3)	−76.30
C10—N2—N4—C20	101.6 (2)	101.98	101.42 (17)	100.85	101.7 (3)	106.11
C21—N6—N8—C31	88.01 (19)	84.55	87.58 (17)	84.91	87.1 (3)	88.25
C21—N6—N8—C35	−86.6 (2)	−89.48	−87.89 (17)	−89.47	−85.9 (3)	−84.60
C25—N6—N8—C31	−88.9 (2)	−90.34	−88.86 (17)	−90.55	−90.4 (3)	−88.06
C25—N6—N8—C35	96.5 (2)	95.61	95.67 (17)	95.05	96.5 (3)	99.08
C26—N7—N9—C36	81.09 (19)	79.99	82.20 (16)	79.81	81.0 (3)	77.06
C26—N7—N9—C40	−93.38 (19)	−93.98	−92.89 (16)	−95.11	−94.1 (3)	−100.56
C30—N7—N9—C36	−102.44 (19)	−104.36	−100.52 (16)	−104.00	−102.1 (3)	−107.33
C30—N7—N9—C40	83.1 (2)	81.65	84.39 (17)	81.06	82.8 (3)	75.03

3.1. Refinement of the GS crystal structure

The refinement of GS was carried out in a standard way and the complete results are summarized in the supplementary material.[1] In Table 2 the most interesting distances and angles compared with results of the refinements of SI and SII are listed. The structures of the two symmetry-independent cations (1) and (2) as well as the arrangement of the two anions and the crystal water are depicted in Fig. 3.

In accordance with Kimura *et al.* (1983) the Ru—N—O linkage is linear with distances of Ru1—N5 = 1.7550 (17), Ru2—N10 = 1.7537 (16), N5—O5 = 1.146 (2), N10—O10 = 1.147 (2) Å and angles of Ru1—N5—O5 = 178.96 (6)°, Ru2—N10—O10 = 175.47 (6)°, which is in the range of all known {RuNO}^{6} compounds (Enemark & Feltham, 1974) with formally Ru^{II} and NO$^+$. The pyridine rings show a propeller-like structure as follows from the torsion angles in Table 3. Note the large displacement ellipsoids of the C atoms in one of the pyridine rings in anion (1) (C11–C15). An alternative rigid-body refinement with only two split molecular positions did not give a significantly better fit even though the number of refined parameters is increased by six. This means that the origin of the observed disorder is, within accuracy of our data collection, a Gaussian distribution of split positions. A similar disorder leading to large displacement ellipsoids is also observed for one of the two PF_6 ions and analogous tests with a split model lead to the same conclusion as for the disordered pyridine ring. These peculiarities remain unaffected when the metastable states are generated and thus we do not consider them further in the discussion. A noticeable fact is that the two negatively charged PF_6 ions are arranged around the formally positively charged NO group. The shortest distances between F and N—O are 2.908 (2) Å for O5, 2.912 (5) Å for N5, 2.801 (2) Å for O10 and 2.898 (2) Å for N10 which is of the order of hydrogen-bond lengths. The N5—O5—F angles with respect to these shortest distances are 104.70 (13) and 116.60 (14)° and those for the second cation are 91.22 (12) and 94.20 (12)°. The shortest distances of the F atoms to the H atoms of the pyridine rings are 2.352 Å (F5—H20), 2.332 Å (F11—H6), 2.292 Å (F16—H28) and 2.243 Å (F21—H1).

3.2. Refinement of the SI crystal structure

The color change of the irradiated sample from orange to pale green and the changes of the lattice constants are clear hints for the formation of the linkage isomer, as already predicted from absorption spectra, IR spectra and

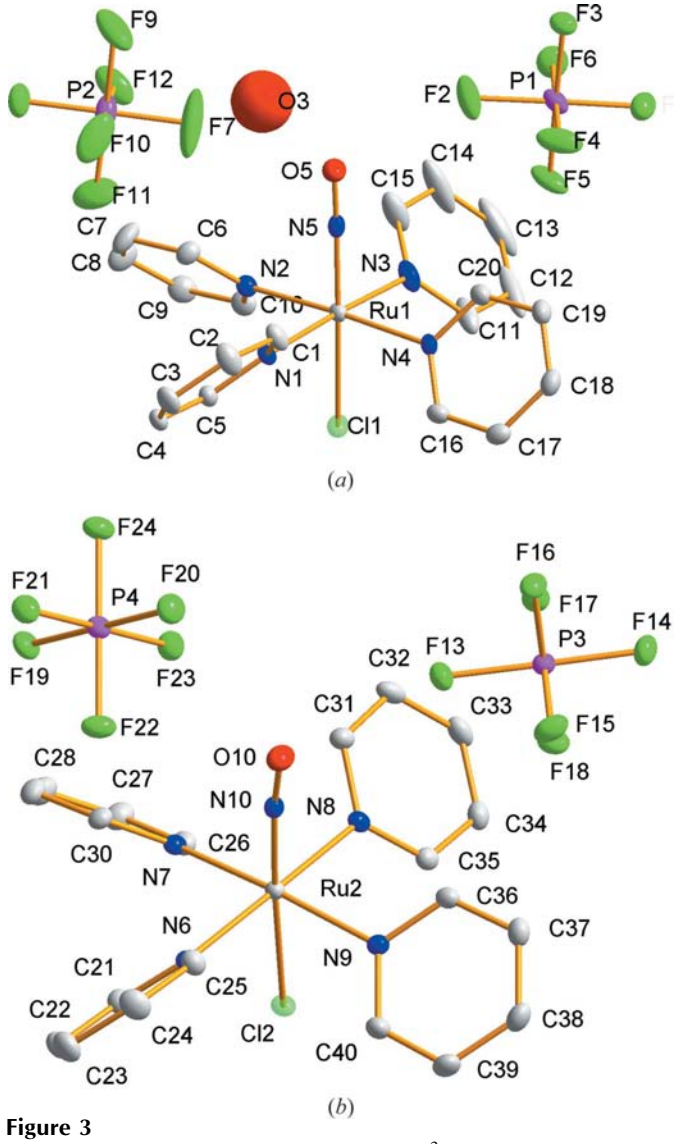

Figure 3
Structure of the two cations $[Ru(py)_4Cl(NO]^{2+}$, the four anions $(PF_6)^-$ and the crystal water H_2O. H atoms are omitted for clarity. The plot is based on the GS refinement.

[1] Supplementary data for this paper are available from the IUCr electronic archives (Reference: CK5038). Services for accessing these data are described at the back of the journal.

the exothermal heat flow during the heating process detected by DSC (Schaniel, Cormary *et al.*, 2007).

The identification of the metastable linkage isomers is usually carried out by inspection of the photodifference maps (Carducci *et al.*, 1997; Schaniel *et al.*, 2005, 2006) which is a difference-Fourier map calculated from structural parameters refined against GS diffraction data with a dataset obtained after illumination. Largest positive and negative regions are then located close to atomic positions which are affected by light irradiation. Such residual electron densities are presented in Figs. 4 and 5. The most pronounced changes (Fig. 4) were observed close to the heavy Ru atoms, where on the side towards the Cl atom a strong positive region is found and on the opposite side towards the N atom a strong negative region is found. This fact is confirmed by the refinement in which a small but very significant shift of the heavy Ru atom towards the Cl atom is found. The residual electron density of the map at the N and O positions (Fig. 5) has a very different character. The density at the N positions is positive and *vice versa* the density at the O positions is negative. This indicates that switching of the N—O group is highly probable. The N—O groups in both molecules were refined as if each atomic position was composed of N and O atoms with corresponding populations of GS and SI. The refined occupancies for the N—O group with the O atom located towards Ru1 and Ru2 were 91.5 (1.6) and 92.8 (1.7)%, so that the average population of SI is $\sim$ 92%. The stability of the refinement and reasonably low standard uncertainties (s.u.) leads to a clear conclusion about the SI population. Both independent molecules gave the same results with good accuracy. Beyond that we tried to refine the remaining 8% in the GS (Ru—N—O) configuration as split positions relative to the Ru—O—N geometry of SI. However, this attempt failed since the atoms of GS and SI, *e.g.* N in GS and O in SI, lie too close together. It is important to note that all intramolecular distances are changed (see Table 2), especially those in the first coordination sphere around the Ru central atom and of the NO ligand. The inversion of the NO ligand leads to a shortening of the distances of the remaining other ligands. Further, the position of Ru with respect to the equatorial plane defined by the equatorial N atoms is significantly changed. In GS it is 0.0592 (2)/0.0741 (2) Å above the equatorial plane in the direction of the N(O) atom while in SI it is only 0.0243 (1)/0.0374 (1) Å above the equatorial plane, such that the planarity is improved, but not completely achieved. While the N—O distance is hardly changed the Ru—O distance in SI is much larger than the Ru—N distance of GS. Thus, the relevant change occurs, as expected, at Ru—N—O. There is a significant influence of the NO inversion on the *trans* Cl ligand. In the two cations, the Ru—Cl distance is shortened in SI by 0.0424/0.0433 Å. Further, all the equatorial Ru—N distances are shortened, such that the pyridine rings move closer to the ruthenium. An interesting observation is the mobility of the pyridine rings. All dihedral angles are changed significantly. The most pronounced difference for the first Ru1 cation occurs for the dihedral angle between the N2 and N3 pyridine rings from 67.62 (6) to 68.49 (7)°, and for the second Ru2 cation for the dihedral angle between the N7 and N9 pyridine rings from 83.51 (6) to 82.47 (7)°. In response to the novel, relaxed electron density distribution in SI all distances in the first and even in the second coordination

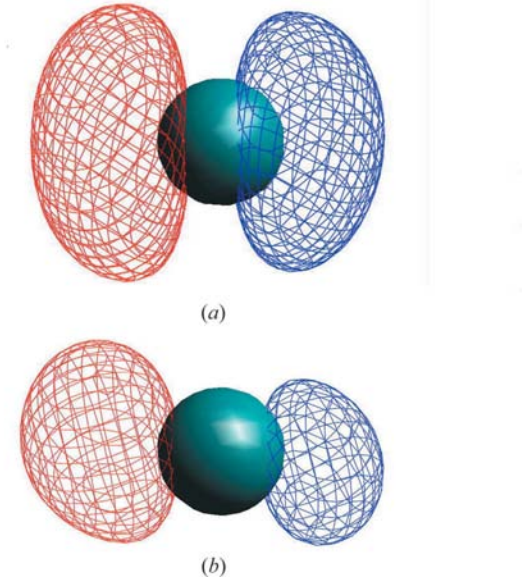

Figure 4
The photodifference maps for SI around the Ru1 and Ru2 atom. The positive (red) and negative (blue) contours are taken at 15 e Å^{-3}.

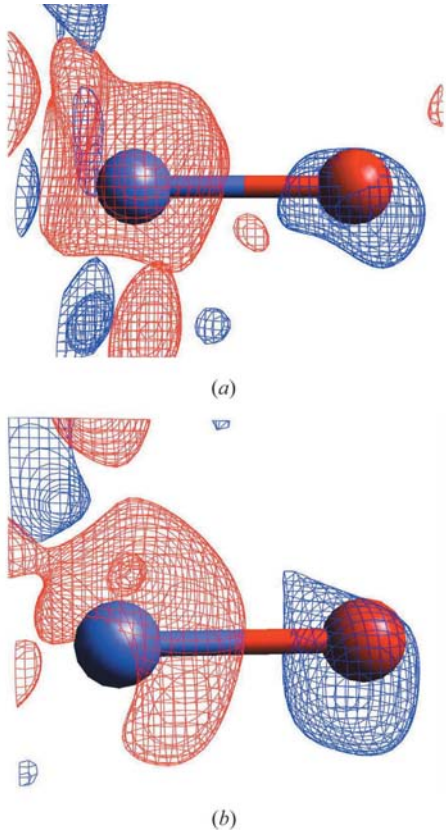

Figure 5
The photodifference maps for SI in the vicinity of N5—O5 and N10—O10. The positive (red) and negative (blue) contours are taken at 1.5 e Å^{-3}.

sphere of the ruthenium central atom including the dihedral angles are changed. Considering the displacement parameters (supplementary material) there is no distinct feature except that the large displacement ellipsoids of the C atoms of the pyridine rings are also present in SI, implying that the above described disorder is not affected by the formation of the metastable states. As in GS the distances of the PF_6 counterions to the N5(O5)/N10(O10) atoms (O in GS) of 2.908 (2)/2.801 (2) Å and 2.876 (2)/2.791 (2) Å are in the range of hydrogen bonds.

3.3. Refinement of the SII crystal structure

As a first step the photodifference-Fourier maps were calculated. These maps, shown in Fig. 6, clearly indicate that in both Ru cations the 90° isomerization takes place and they could be used to localize N and O atoms in the SII configuration. Moreover, local densities at the GS positions of the N—O group are negative and of the same order as the positive perpendicular maxima. The amount of electron densities for the two N—O ligands are different, which is a clear hint of different populations in the two cations. All these facts were used to prepare a starting model for subsequent refinement.

For each Ru cation the sum of occupancies of both N—O configurations were constrained to the full occupancy. For all N—O atoms only isotropic ADPs (atomic displacement parameters) were used as the non-fully occupied positions contributed little to the structure factors and moreover the number of observed reflections [$I > 3\sigma(I)$] was considerably smaller than those for GS and SI data collection (see Table 1). The occupancies of the SII configuration were found to be 35.0 (13)% and 60.2 (9)% for the Ru1 and Ru2 cation, respectively, with a large error margin and a mean value of $\sim$ 48%. The value of GOF(all) < 1, given in Table 1, clearly indicates an overestimated structure model (766 refined parameters, 4000 observed reflections). Consequently, the refined structure of SII is regarded only as a first step in order to determine the main features of the light-induced structural changes.

All refined data are given in the supplementary material. In Fig. 7 the structures of the two cations in the mixed-state SII + GS are depicted, as obtained after irradiation with λ = 980 nm. Both states (GS and SII) are drawn on the same molecule. Owing to the nearly 90° position of the N—O ligand, both atoms are now bonded to the Ru central atom. The relevant distances are presented in Table 2. With respect to GS, the Ru—N distances are increased and also the Ru—O bond lengths are larger than in SI. The N—O bond lengths are significantly decreased owing to the fact that now N and O are bonded to Ru, which results in the down shift of the ν(N—O) stretching vibrations of $\sim$ 300 cm^{-1} (Schaniel, Cormary *et al.*, 2007). The limited number of observed reflections does not allow for a refinement of all structural details. However, the main structural features of SII are clearly revealed, as was tested by restraining the N—O distances to a value of $\sim$ 1.15 Å. This refinement yielded the same results within error as obtained for unrestricted N—O distances. The N—O ligand in SII is in the eclipsed configuration, *i.e.* N and O are positioned above the connection line between N atoms of the pyridine rings and the central Ru atom. Interestingly, the Cl—Ru—O angles (171.5/173.18°) and the Cl—Ru—N angles (158.4/160.8°) reveal that the N atoms are shifted out of the almost linear Cl—Ru—N—O direction and the O atoms are now lying in the almost linear Cl—Ru—O direction. As in SI, besides the changes of the Ru—N—O moiety the distance of the *trans* ligand to Ru is affected in SII. The Ru—Cl distance is 2.3045 (8)/2.2966 (8) Å and thus 0.0161/0.0265 Å shorter compared with GS. The Ru—N(py) distances are systematically shortened and the dihedral angles are changed.

The analysis of SII reveals problems which are common in the refinement of mixed structures due to the neighboring positions of the N and O atoms. The reason is the presence of 65% or 39.8% of GS molecules. Short distances between partly occupied positions of N—O atoms together with specific and generally different ADP ellipsoids would need a more accurate data set for detailed structure analysis. Nevertheless, the SII geometry has been unambiguously determined.

4. Simulation of influence of the SI/GS occupancy

As mentioned above for the studied compound a very high population (about 92%) of the SI state has been achieved and

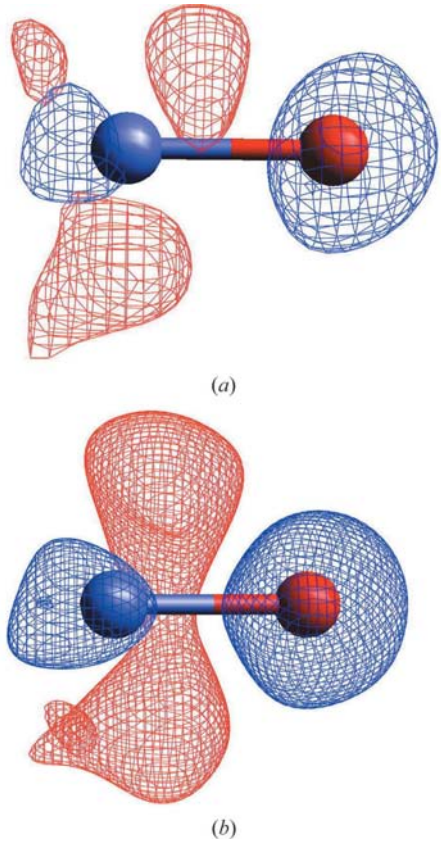

Figure 6
The photodifference maps for SII in the vicinity of N5—O5 and N10—O10. The positive (red) and negative (blue) contours are taken at 1.2 e $Å^{-3}$.

Table 4
Main characteristics of refinements against simulated data sets for the split-atom model.

Simulated SI occupancy	10%	20%	30%	40%	50%	60%	70%	80%	90%
SI–Ru1 occupancy (%)	10.0 (9)	20.2 (9)	30.5 (9)	38.8 (9)	47.4 (9)	60.1 (9)	69.4 (9)	80.1 (9)	89.1 (9)
Ru1—O5	1.92 (3)	1.91 (3)	1.89 (2)	1.90 (2)	1.90 (2)	1.91 (2)	1.92 (1)	1.904 (5)	1.903 (6)
Ru1—N5′	1.792 (3)	1.792 (7)	1.80 (1)	1.81 (2)	1.81 (2)	1.79 (3)	1.77(2)	1.82 (3)	1.86 (6)
Ru1—Cl1	2.37 (3)	2.34 (4)	2.25 (2)	2.26 (2)	2.27 (2)	2.32 (2)	2.312 (6)	2.270 (4)	2.287 (3)
Ru1—Cl1′	2.300 (3)	2.294 (9)	2.323 (8)	2.32 (1)	2.32 (2)	2.24 (3)	2.22 (1)	2.32 (2)	2.19 (2)
N5—O5	1.18 (4)	1.16 (6)	1.23 (3)	1.28 (3)	1.12 (4)	1.14 (2)	1.16 (1)	1.150 (9)	1.169 (7)
N5′—O5′	1.159 (4)	1.16 (1)	1.13 (1)	1.15 (2)	1.19 (3)	1.18 (4)	1.17 (3)	1.19 (4)	1.06 (6)
SI–Ru2 occupancy (%)	8.4 (9)	20.1 (9)	30.5 (9)	40.1 (9)	49.4 (9)	60.4 (9)	69.9 (9)	80.9 (9)	89.5 (8)
Ru2—O10	1.90 (4)	1.89 (3)	1.89 (2)	1.88 (2)	1.88 (2)	1.89 (1)	1.921 (6)	1.899 (5)	1.900 (5)
Ru2—N10′	1.797 (4)	1.800 (9)	1.801 (11)	1.83 (2)	1.83 (2)	1.83 (2)	1.75 (2)	1.84 (3)	1.92 (6)
Ru2—Cl2	2.34 (2)	2.35 (1)	2.31 (1)	2.35 (1)	2.28 (2)	2.32 (1)	2.271 (7)	2.267 (4)	2.283 (3)
Ru2—Cl2′	2.305 (2)	2.293 (3)	2.296 (6)	2.26 (1)	2.30 (2)	2.24 (2)	2.32 (2)	2.34 (2)	2.23 (3)
N10—O10	1.16 (12)	1.17 (4)	1.15 (4)	1.19 (2)	1.19 (2)	1.17 (1)	1.18 (1)	1.171 (9)	1.161 (7)
N10′—O10′	1.155 (9)	1.15 (1)	1.16 (2)	1.14 (2)	1.13 (2)	1.14 (2)	1.11 (3)	1.10 (4)	1.09 (7)
R	0.0171	0.0171	0.0172	0.0171	0.0171	0.0172	0.0171	0.0171	0.0171

therefore the refined positions should be almost unaffected by the coexistence of GS and SI. Therefore, the question arose as to whether the sensitivity of the structure refinement was sufficient to study this type of tiny detail in the electron density and how different SI occupancies could modify refined positions with respect to the pure SI, and if a split model can recover correct distances for both configurations. To test for this, a simulation procedure based on different mixing of 'idealized' SI and GS models has been used. The 'idealized' GS model uses all parameters as refined from the GS dataset except for N5, O5, N10, O10, Cl1 and Cl2, which were shifted to the positions calculated by DFT. Similarly the 'idealized' SI model was built from the set of refined GS parameters, but now the groups N5—O5, N10—O10 were switched from Ru—N—O to Ru—O—N coordination and their distances were modified, as predicted by DFT. Analogical modifications were applied to Cl atoms. The Ru atoms were kept in the GS position in spite of the fact that a small positional shift, as mentioned above, has been detected in SI. However, this shift has a strong influence on structure factors, but the influence on the geometry is not substantial. Thus, the mixing of SI and GS from 0 to 100% with steps of 10% is simulated through the occupancies of the atoms O5/N5′, N5/O5′, O10/N10′, N10/O10′, Cl1/Cl1′ and Cl2/Cl2′. The primes indicate atomic positions of the 'idealized' GS. These parameters were used to generate 11 artificial sets of structures factors within the resolution limit $\sin\theta/\lambda \simeq 0.8$ Å^{-1}. During the generation process noise similar to that observed for real data collection was modeled by a random procedure and combined with calculated structure factors.

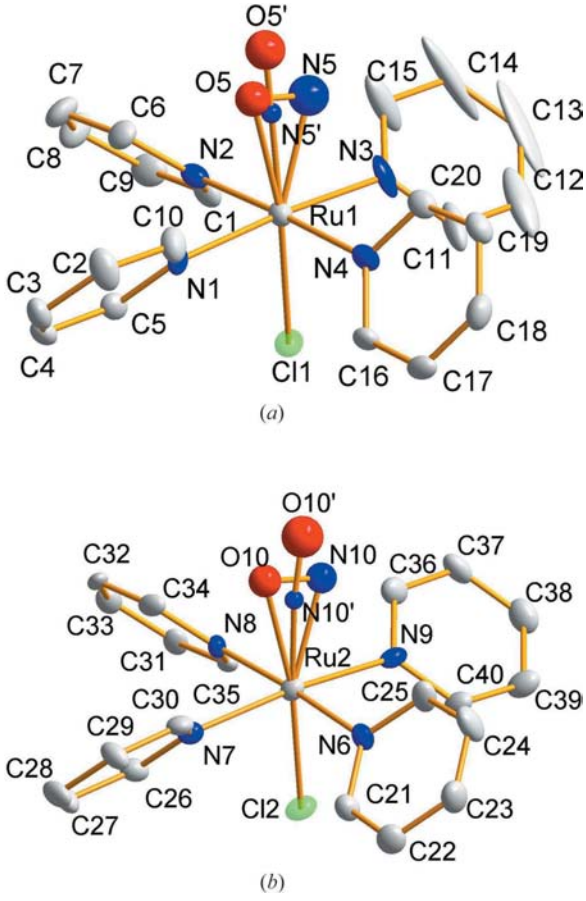

Figure 7
Structure of the two cations in the mixed states GS and SII. The ADPs are plotted at the 50% probability level including those described isotropically.

First attempts, in which all ADPs were refined independently, led to strong correlations and singularities between parameters of split atoms, even for occupancies close to 50% where the chance to refine such a model is maximal. Therefore, restrictions keeping ADPs identical for split positions were applied in all subsequent refinements. This assumption means that different atoms, *e.g.* N and O, in a similar coordination environment, *e.g.* inner or outer position with respect to Ru, have the same ADPs. Then the refinements of split-atom models slowly converged for all data sets, except zero and fully populated ones. The refined values did not deviate

Table 5
Main characteristics of refinements against simulated data sets for the restricted position model.

Simulated SI occupancy	0%	10%	20%	30%	40%	50%	60%	70%	80%	90%	100%
SI–Ru1 occupancy (%)	−1.4 (9)	10.3 (9)	19.6 (9)	29.9 (9)	41.1 (9)	50.1 (9)	61.8 (9)	72.0 (9)	80.4 (9)	89.6 (9)	99.1 (9)
Ru1—N5/O5′	1.7845 (6)	1.7964 (6)	1.8079 (6)	1.8220 (6)	1.8361 (6)	1.8463 (6)	1.8582 (6)	1.8695 (6)	1.8804 (5)	1.8907 (5)	1.9001 (5)
$U_{\parallel}$(N5/O5′)	0.0198 (2)	0.0216 (2)	0.0229 (2)	0.0232 (2)	0.0233 (2)	0.0235 (2)	0.0238 (2)	0.0228 (2)	0.0213 (2)	0.0211 (2)	0.0197 (2)
Ru1—Cl1/Cl1′	2.3388 (2)	2.3345 (2)	2.3310 (2)	2.3267 (2)	2.3228 (2)	2.3185 (2)	2.3150 (2)	2.3109 (2)	2.3072 (2)	2.3028 (2)	2.2993 (2)
$U_{\parallel}$ (Cl1/Cl1′)	0.01347 (7)	0.01377 (7)	0.01377 (7)	0.01407 (7)	0.01390 (7)	0.01391 (7)	0.01401 (7)	0.01384 (7)	0.01389 (7)	0.01375 (7)	0.01367 (7)
N—O	1.1509 (9)	1.1497 (9)	1.1449 (9)	1.1431 (9)	1.1404 (9)	1.1424 (9)	1.1407 (9)	1.1429 (10)	1.1456 (9)	1.1479 (10)	1.1515 (9)
SI–Ru2 occupancy (%)	−0.7 (9)	10.4 (9)	20.8 (9)	29.3 (9)	41.5 (9)	48.9 (9)	59.8 (9)	70.9 (9)	81.3 (9)	89.8 (8)	101.0 (8)
Ru2—N10/O10′	1.7835 (6)	1.7960 (6)	1.8078 (6)	1.8231 (6)	1.8337 (6)	1.8465 (6)	1.8579 (5)	1.8692 (5)	1.8803 (5)	1.8906 (5)	1.8995 (5)
$U_{\parallel}$ (N10)	0.0158 (2)	0.0173 (2)	0.0188 (2)	0.0192 (2)	0.0194 (2)	0.0195 (2)	0.0195 (2)	0.0193 (2)	0.0181 (2)	0.0173 (2)	0.0162 (2)
Ru2—Cl2/Cl2′	2.3387 (2)	2.3350 (2)	2.3307 (2)	2.3270 (2)	2.3230 (2)	2.3191 (2)	2.3147 (2)	2.3109 (2)	2.3072 (2)	2.3032 (2)	2.2992 (2)
$U_{\parallel}$ (Cl2/Cl2′)	0.01100 (6)	0.01113 (6)	0.01145 (6)	0.01143 (6)	0.01140 (6)	0.01146 (6)	0.01140 (6)	0.01134 (6)	0.01133 (6)	0.01125 (6)	0.01107 (6)
N—O	1.1516 (8)	1.1490 (8)	1.1468 (8)	1.1415 (8)	1.1423 (8)	1.1407 (8)	1.1435 (8)	1.1440 (8)	1.1456 (8)	1.1485 (8)	1.1513 (8)
R	0.0171	0.0172	0.0171	0.0173	0.0171	0.0171	0.0172	0.0172	0.0172	0.0171	0.0171

significantly from those used to build the models (see Table 4). However, the s.u. values of distances were relatively large especially for atoms belonging to less occupied models. The high s.u. values for Cl atoms did not allow any conclusion about real GS and SI distances to Ru atoms.

An alternative way to refine the SI structure is to use a restricted position model in which SI and GS positions are constrained to have the same positions and ADPs, *i.e.* effectively one refines a single molecule with respect to position and ADPs but two with respect to the occupation of states (SI and GS). Thus, the refined positions and ADPs for the molecule correspond to those of a hybrid molecule consisting of SI and GS states (Schaniel *et al.*, 2006). Such refinements are very stable and the s.u.s of atomic positions are considerably reduced. The R values of the fit (see Table 5) are not different in spite of the fact that the number of refined parameters is lower.

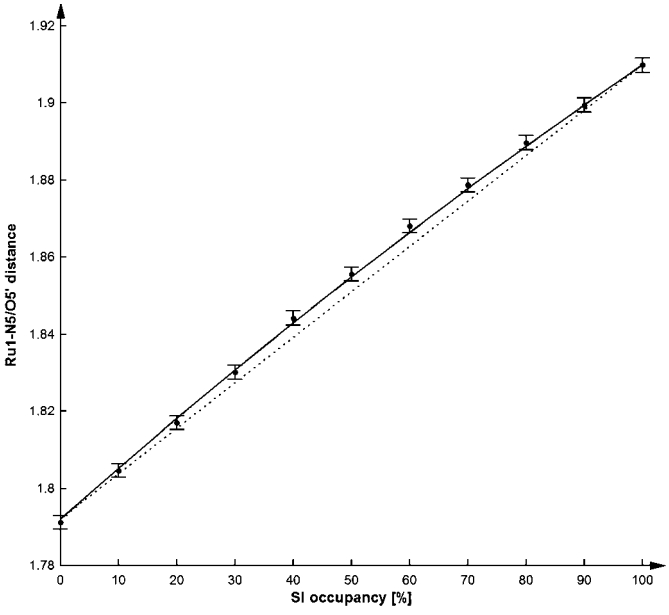

Figure 8
Ru1—N5/O5′ distances as a function of occupation. The dotted line shows a linear function of GS and SI distances.

On the other hand, the refined positions are moving towards an effective center of split atoms. One question remains about if a more precise conclusion about Ru—O distances in SI can be drawn from Ru—O as found from the refinement against simulated data for different SI occupancies. The distance Ru—O5/N5′ as a function of occupancy is presented in Fig. 8. As a first approximation, we can just use a linear function (dotted line) between the 'ideal' GS Ru—N distance and the 'ideal' Ru—O distance. This function does not follow the refined points very well. A more realistic description can be achieved taking into account the fact that the split atom is composed of atoms having different local electron density. The simplest model with weights proportional to the number of electrons leads to the formula

$$d(x) = \frac{d_{\rm SI} Z_1 x + d_{\rm GS} Z_2 (1 - x)}{Z_2 + (Z_1 - Z_2)x}, \qquad (2)$$

where Z_1 and Z_2 are the atomic numbers of split atoms, $d_{\rm GS}$ and $d_{\rm SI}$ are the 'ideal' distances to the central atom for GS and SI, respectively, and x is the fractional occupancy of the second configuration. Note that the formula for the case $Z_1 = Z_2$ reduces to the simple linear function. Equation (2) can be used to obtain a more realistic distance for SI from the refined value and that known for GS.

Another influence of mixing GS and SI is visible from the dependence of the N—O distance on the actual SI occupancy (see Table 4). This distance, being in the simulated model identical for GS and SI, is shortened considerably for occupancies of $\sim 50\%$ as a result of the mutual shift of both atoms.

As mentioned above the harmonic ADPs for split atoms should also be affected by the fact that the refined position represents a split position. In Fig. 9 the projection of harmonic ADPs of the O5 atom in the Ru1—O5 bond as a function of SI occupancy is presented. It is obvious that the broadening is present especially for occupancies close to 0.5 as expected.

5. DFT calculations for the solid state

DFT calculations were performed with the program package *DMol*^{3} (Delley, 1990). This method allows the study of vacuum boundary conditions for gas-phase molecules as well as bulk crystal band structures. Furthermore, surface slab models can be treated with the same basis sets and other details of the method kept consistent (Delley, 2000). The present calculations were carried out using the PBE functional (Perdew *et al.*, 1996). Variational numerical local orbitals basis sets at the level of the default DND (Delley, 1990) were used. These numerical basis sets are constructed with an atomic response idea in mind. They were demonstrated to represent a wide class of systems. DND does not include a *p*-polarization function on the H atoms, and is thus a moderately less accurate basis set than the DNP. However, the H atoms are somewhat peripheral to our present focus on the Ru—N—O bonds, where only a minor influence of the *p*-polarization functions on H atoms is seen for the properties of interest. For the Ru atom, scalar relativistic effects were included *via* a pseudo-potential (Delley, 2002). Expedient calculations of the electrostatics involve an auxiliary density as usual (Delley, 1990). The auxiliary density for transition metal elements, open *d* shells, is truncated at $L = 4$ multipolar components. For other elements the auxiliary density goes up to octupoles except for H, where truncation is at quadrupoles according to the default settings of *DMol*^{3}.

The K-point sampling for the crystalline compounds is with a $2 \times 2 \times 2$ mesh containing the Γ point. Overall, the present method has been demonstrated to be in excellent agreement for the ground-state energetics of molecules in a large database (Delley, 2006). The corresponding energy surface gives an excellent account of structural and vibrational properties of other nitrosyl compounds (Delley, 2008).

The PBE functional has a tendency to result in slightly lengthened bonds (usually 0–0.04 Å). A similar but smaller effect of lengthening the bonds comes from limitations of the DND basis set by 0–0.01 Å. All calculations were performed at a temperature of $T = 0$ K and for 100% population of SI and SII. The geometry optimizations were started from the positions determined by the X-ray diffraction experiments. Cell parameters were not optimized as these are mostly dependent on weak intermolecular interactions for which expectations of the accuracy of the electronic structure calculations are low. The calculations would not provide a sharp prediction for the photo-induced change on the lattice parameter. The intramolecular predictions were computationally well defined, with an expected numerical uncertainty for covalent bond lengths below 0.01 pm. The convergence criterion for the geometry optimization was that the maximum gradient on any atom did not exceed 0.0003 Hartree/a_0 and that the total energy change from the previous geometry step remained smaller than 1 μHartree per unit cell.

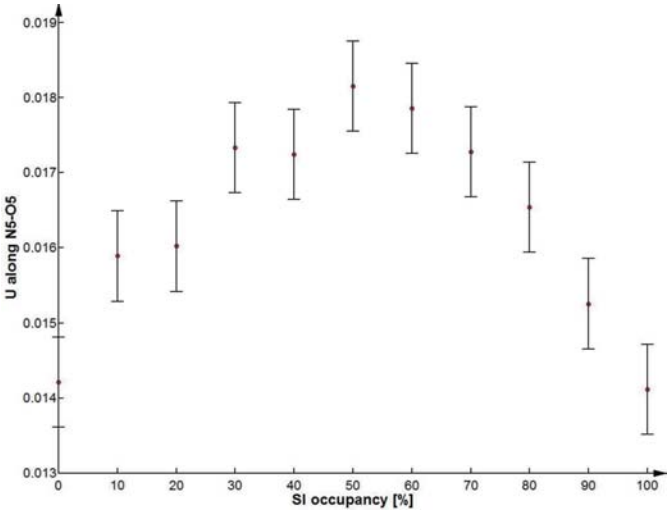

Figure 9
The projection of harmonic ADPs (Å^2) of the O5 atom onto the Ru—O5 bond as a function of SI occupancy.

The calculated structure for the ground state agreed very well with the experimentally determined structure, as presented in the supplementary material and for selected distances and angles in Tables 2 and 3. All the calculated bond lengths are in general between 0.01 and 0.04 Å too long, which can be expected from the used functional PBE. Especially the Ru1—N5/Ru2—N10 and N5—O5/N10—O10 bond lengths agree within 0.04 Å with the X-ray data. The maximum deviation between calculated and refined angles in Table 2 is 0.38° for Cl2—Ru2—N10. All other angles in Table 2 and especially the torsion angles in Table 3 agree within 0.18–3.64° of the experimentally determined ones. The torsion angles have very low force constants, which makes their calculation quite difficult.

As for the ground state the DFT calculations for SI reproduce again all the observed distances and angles with high accuracy up to the second digit. Complete listings of calculated structural data are presented in the supplementary material and selected bond lengths are given in Tables 2 and 3. All the trends of bond shortening and changes in angles when going from GS to SI are predicted by the calculation. Note that all the calculated distances are systematically larger by 0.01–0.05 Å compared with the refined data. The largest deviations between calculated and refined data are found for the Ru1—O5 and Ru1—N3 distances, being 0.037 and 0.041 Å longer, compared with the refined values. Interestingly, a small but significant shortening of the N—O bond length is also found by the DFT calculations, which however cannot explain the dramatic shift of the ν(N—O) stretching vibration by ~ 110 cm^{-1} to lower frequencies. The Ru—N—O and Ru—O—N angles are nearly the same, which means that the 180° rotation of the N—O ligand does not change the symmetry of the molecule. The largest difference of 1.79° appears for the Ru2—O10—N10 angle, whereby the corresponding Ru1—N5—O5 angle has a smaller difference of 0.92°. Again, the torsion angles with their low force constants deviate between 0.2 and 3.48° (Table 3) from the measured data.

Owing to the low population of 48% of the metastable state SII has to be considered in a special way. Due to the good agreement between the measured and calculated bond lengths

and angles of GS and SI, we can assume that the calculated data of SII reproduce this structure with high accuracy. The calculation was carried out for a population of 100% so that a larger difference between the presented data is expected. This is clearly seen, *e.g.* in the N—O distances where the X-ray data are shorter by 0.1–0.2 Å. The reduced data set of SII excludes a deeper discussion.

6. Discussion and conclusion

As a fundamental result we can state that the refinement of photogenerated states and especially NO linkage isomers can be performed with high accuracy if the population is high enough. In $[Ru(py)_4Cl(NO)](PF_6)_2{\cdot}0.5H_2O$ the photogeneration of NO linkage isomers leads to a change of atomic distances of all atoms in the first coordination sphere of the central Ru atom besides the NO ligand. Also, the dihedral angles of the pyridine ligands adapt to the new configuration owing to the new electron density distribution at the ruthenium. The residual electron densities in the photodifference maps give a clear hint for the positions of atoms in the following refinements.

The detailed analysis of the atomic distances as a function of the population of the metastable species shows that for populations below 50% only qualitative statements can be made. Absolute values for distances will be distorted by the presence of the ground-state configuration. Consequently, a simple application of equation (1) with all the necessary constraints will show the structural behavior in photocrystallography in a qualitative way. This is confirmed in a comprehensive analysis of the bond lengths on the population for spin-crossover compounds by Legrand *et al.* (2007).

In order to check the stability of the refinement we have generated several simulations with different SI occupancies to prove that the refinement method can correctly reproduce the starting model. In all simulations we could correctly (within s.u.) reproduce the starting occupancies. The refinement was also stable for reduced diffraction angle.

The comparison of calculated and experimentally determined parameters for GS and SI shows that the DFT calculation for the solid state reached a high level of accuracy. Deviations for bond lengths are of the order 0.01–0.05 Å. Compared with the calculations of the free ion (Schaniel, Cormary *et al.*, 2007), the distances and angles of the calculations for the solid state with eight molecules per unit cell yield results which are significantly closer to the experimental values.

The difference in populations for powder samples (Schaniel, Cormary *et al.*, 2007) and single crystals is most probably induced by the difference in mutual orientation between light-polarization and the M—N—O axis, as is known from detailed absorption studies on $Na_2[Fe(CN)_5NO]{\cdot}2H_2O$ (Schaniel *et al.*, 2002). From these measurements it is also known that the absorption cross sections for SII are much more sensitive to the polarization than those of GS and SI (Schaniel *et al.*, 2002), which could explain the fact that the two molecules exhibit different amounts of SII populations.

Combining the shortening of the N—O bond length in SI by 0.006/0.005 Å with a decrease in the ν(N—O) vibration of 143 cm^{-1} we can explain the shift of the ν(N—O) vibration by an increase of the electron density on the NO ligand. In a simple picture of a harmonic oscillator one would expect from the decrease of the vibration a significant increase of the bond length, which is not the case. However, going from NO^+ to NO^0 the ν(N—O) frequency decreases, so that a little increase of the charge on the NO can explain the vibrational behavior in SI.

This work was supported by the Deutsche Forschungsgemeinschaft (WO618/8–1), Rheinisches Institut für Umweltforschung at the University of Köln and by the Czech Science Foundation grant number 202/07/J007.

References

Becker, P. J. & Coppens, P. (1974). *Acta Cryst.* A**30**, 129–147.
Bitterwolf, T. E. (2004). *J. Photochem. Photobiol. A*, **163**, 209–213.
Bottomley, F. & Mukaida, M. (1982). *J. Chem. Soc. Dalton Trans.* pp. 1933–1937.
Bowes, K. F., Cole, J. M., Husheer, S. L. G., Raithby, P. R., Savarese, T. L., Sparkes, H. A., Teat, S. J. & Warren, J. E. (2006). *Chem. Commun.* **23**, 2448–2450.
Brandenburg, K. & Putz, H. (2005). *DIAMOND*, Version 3.0c. Crystal Impact GbR, Bonn, Germany.
Bressler, C., Abela, R. & Chergui, M. (2008). *Z. Kristallogr.* **223**, 307–321.
Carducci, M. D., Pressprich, M. R. & Coppens, P. (1997). *J. Am. Chem. Soc.* **119**, 2669–2678.
Cole, J. M. (2004). *Chem. Soc. Rev.* **33**, 501–513.
Collet, E., Buron-Le Cointe, M., Lorenc, M. & Cailleau, H. (2008). *Z. Kristallogr.* **223**, 272–282.
Coppens, P., Novozhilova, I. & Kovalevsky, A. (2002). *Chem. Rev.* **102**, 861–884.
Coppens, P., Zheng, S.-L. & Gembicky, M. (2008). *Z. Kristallogr.* **223**, 265–271.
Delley, B. (1990). *J. Chem. Phys.* **92**, 508–517.
Delley, B. (2000). *J. Chem. Phys.* **113**, 7756–7764.
Delley, B. (2002). *Phys. Rev. B*, **66**, 155125.
Delley, B. (2006). *J. Phys. Chem. A*, **110**, 13632–13639.
Delley, B. (2008). *Z. Kristallogr.* **223**, 329–333.
Delley, B., Schefer, J. & Woike, Th. (1997). *J. Chem. Phys.* **107**, 10067–10074.
Enemark, J. H. & Feltham, R. D. (1974). *Coord. Chem. Rev.* **13**, 339–406.
Fomitchev, D. V., Bagley, K. A. & Coppens, P. (2000). *J. Am. Chem. Soc.* **122**, 532–533.
Grenthe, I. & Nordin, E. (1979). *Inorg. Chem.* **18**, 1869–1874.
Gütlich, P., Garcia, Y. & Woike, Th. (2001). *Coord. Chem. Rev.* **219**, 839–879.
Gütlich, P., van Kroningsbruggen, P. J. & Renz, F. (2004). *Struct. Bond.* **107**, 27–75.
Hauser, A. (1991). *Coord. Chem. Rev.* **111**, 275–290.
Ishikawa, T. & Tanaka, K. (2008). *Z. Kristallogr.* **223**, 334–342.
Kimura, T., Sakurai, T., Shima, M., Togano, T., Mukaida, M. & Nomura, T. (1983). *Inorg. Chim. Acta*, **69**, 135–140.
Korff Schmising, C. von, Bargheer, M., Woerner, M. & Elsaesser, T. (2008). *Z. Kristallogr.* **223**, 283–291.
Kovalevsky, A. Y., King, G., Bagley, K. A. & Coppens, P. (2005). *Chem. Eur. J.* **11**, 7254–7264.
Kubota, M. & Ohba, S. (1992). *Acta Cryst.* B**48**, 627–632.

Legrand, V., Carbonera, C., Pillet, S., Souhassou, M., Letard, J.-F., Guionneau, P. & Lecomte, C. (2005). *J. Phys.* **21**, 73–80.
Legrand, V., Pillet, S., Weber, H.-P., Souhassou, M., Létard, J.-F., Guionneau, P. & Lecomte, C. (2007). *J. Appl. Cryst.* **40**, 1076–1088.
Nakanishi, H., Jones, W., Thomas, J. M., Hursthouse, M. B. & Motevalli, M. (1981). *J. Phys. Chem.* **85**, 3636–3642.
Nasu, K. (2004). Editor. *Photoinduced Phase Transitions.* Singapore: World Scientific Publishing Co. Pte. Ltd.
Ookubo, K., Morioka, Y., Tomizawa, H. & Miki, E. (1996). *J. Mol. Struct.* **379**, 241–247.
Oxford Diffraction (2007*a*). *CrysAlis CCD*. Oxford Diffraction, Abingdon, Oxfordshire, England.
Oxford Diffraction (2007*b*). *CrysAlis RED*. Oxford Diffraction, Abingdon, Oxfordshire, England.
Perdew, J. P., Burke, K. & Ernzerhof, M. (1996). *Phys. Rev. Lett.* **77**, 3865–3868.
Petříček, V., Dušek, M. & Palatinus, L. (2006). *JANA*2006. Institute of Physics, Praha, Czech Republic.
Pillet, S., Legrand, V., Weber, H.-P., Souhassou, M., Letard, J.-F., Guionneau, P. & Lecomte, C. (2008). *Z. Kristallogr.* **223**, 235–249.
Pressprich, M. R., White, M. A., Vekhter, Y. & Coppens, P. (1994). *J. Am. Chem. Soc.* **116**, 5233–5238.
Rachford, A. A., Petersen, J. L. & Rack, J. J. (2005). *Inorg. Chem.* **44**, 8065–8075.
Schaniel, D., Cormary, B., Malfant, I., Valade, L., Woike, Th., Delley, B., Krämer, K. & Güdel, H. U. (2007). *Phys. Chem. Chem. Phys.* **9**, 3717–3724.
Schaniel, D., Schefer, J., Delley, B., Imlau, M. & Woike, Th. (2002). *Phys. Rev. B*, **66**, 085103.
Schaniel, D., Woike, Th., Delley, B., Biner, D., Krämer, K. & Güdel, H. U. (2007). *Phys. Chem. Chem. Phys.* **9**, 5149–5157.
Schaniel, D., Woike, Th., Schefer, J. & Petříček, V. (2005). *Phys. Rev. B*, **71**, 174112.
Schaniel, D., Woike, Th., Schefer, J., Petricek, V., Krämer, K. & Güdel, H. U. (2006). *Phys. Rev. B*, **73**, 174108.
Schefer, J., Schaniel, D., Petříček, V. & Woike, Th. (2008). *Z. Kristallogr.* **223**, 259–264.
Sizova, O. V., Lubimova, O. O., Sizov, V. V. & Ivanova, N. V. (2008). *Z. Kristallogr.* **223**, 343–355.
Sheldrick, G. M. (2008). *Acta Cryst.* A**64**, 112–122.
Varret, F., Boukheddaden, K., Goujon, A., Gillon, B. & McIntyre, G. J. (2008). *Z. Kristallogr.* **223**, 250–258.
Werner, A. (1907). *Ber. Dtsch. Chem. Ges.* **40**, 765–788.
Zöllner, H., Krasser, W., Woike, T. & Haussühl, S. (1989). *Chem. Phys. Lett.* **161**, 497–501.